Orientational Tuning of Monolayers of Amphiphilic Ruthenium(II) Complexes for Optimizing Chirality Distinction Capability

Kenji Tamura,*,† Hisako Sato,‡,§ Satoko Yamashita,‡ Akihiko Yamagishi,‡,§ and Hirohisa Yamada†

Ecomaterials Center, National Institute for Materials Science, 1-1 Namiki, Tsukuba, Ibaraki, 305-0044 Japan, Department of Earth and Planetary Science, Graduate School of Science, The University of Tokyo, Hongo, Tokyo 113-0033, Japan, and CREST, Japan Science and Technology Agency (JST)

Received: February 13, 2004; In Final Form: April 19, 2004

The following six types of Ru(II) complexes were synthesized with an aim to develop a monolayer with chiral discrimination: **1** $[Ru(bpy)_2(4\text{-}C11bpy)](ClO_4)_2$ (bpy = 2,2′-bipyridine, 4-C11bpy= 4-methyl-4′-undecyl-2,2′-bipyridine); **2** $[Ru(bpy)_2(4,4'\text{-}dC11bpy)](ClO_4)_2$ (4,4′-dC11bpy = 4,4′-diundecyl-2,2′ -bipyridine); **3** $[Ru(bpy)_2(5\text{-}C11bpy)](ClO_4)_2$ (5-C11bpy= 5-methyl-5′-undecyl-2,2′-bipyridine); **4** $[Ru(bpy)_2(5,5'\text{-}dC11bpy)](ClO_4)_2$ (5,5′-dC11bpy = 5,5′-diundecyl-2,2′-bipyridine); **5** $[Ru(bpy)_2(4\text{-}C18bpy)](ClO_4)_2$ (4-C18bpy= 4-methyl-4′-octadecyl-2,2′-bipyridine); **6** $[Ru(bpy)_2(4,4'\text{-}dC18bpy)](ClO_4)_2$ (4,4′-dC11bpy = 4,4′-dioctadecyl-2,2′-bipyridine). These complexes possess one or two alkyl chains at 4,4′- or 5,5′-positions of the 2,2′-bipyridine ligand. A traditional amphiphile is a linear molecule with a polar head attached by one or two alkyl chains, whereas the present complexes cover both traditional (**1**, **2**, **5**, and **6**) and nontraditional amphiphilic molecules (**3** and **4**). The monolayer behavior of these Ru(II) complexes on a subphase of 0.1 M $NaClO_4$ aqueous solution was compared using surface pressure−molecular area ($\pi-A$) isotherm measurements and Brewster angle microscopy (BAM) observations. The vertical structure of monolayers deposited onto a silicon substrate was characterized with X-ray reflectivity (XRR) measurements. Chirality effects were investigated using two procedures: one was to compare the $\pi-A$ isotherms between a racemic mixture and a pure enantiomer and the other to observe the effect of chiral anions in the subphase. As a result, complex **4** ($[Ru(bpy)_2(5,5'\text{-}dC11bpy)](ClO_4)_2$), belonging to the nontraditional group, was the only molecule with a distinct chirality discrimination capability toward the chiral anion, bis[(+)-tartrato][diantimonato(III)]dipotassium, $K_2[Sb_2(+)\text{-}(C_4H_2O_6)_2]$. The observed chiral distinction of this molecule was interpreted in terms of a preferential orientation of the polar head with respect to the aqueous phase.

1. Introduction

Chirality effects in a floating monolayer have been investigated using two different approaches. One approach compares monolayer behavior between a racemic mixture and an enantiomer. This reveals the effects of chirality on the stacking of amphiphiles at an air−water interface, represented by homochiral or heterochiral interactions at the two extremes. The chiral discrimination is manifested in the shape and characteristic features of the $\pi-A$ isotherms. Using this approach, Arnett et al. have revealed a large chirality effect on the monolayer formation of amino acid derivatives.[1] The second approach is to observe the monolayer behavior in response to the adsorption of a chiral molecule in a subphase or in air. An attempt has been made to mimic the functionality of biological membranes, such as highly selective transport or inclusion of chiral solutes through cell membranes. The investigation is important to develop molecular devices for practical applications, such as chemical sensors.[2−10] For example, Vodyanoy et al. have elucidated the chiral recognition in enantiomeric molecules of an odorant carvone by phospholipid monolayers.[11] The authors of this study have also reported studies on the chiral recognition of amphiphilic Ru(III) complexes at an air−water interface.[12]

In both of the approaches outlined above, the systematic tuning of the amphiphilic molecule is a key step to optimize such chirality effects. In the traditional concept, the polar or charged hydrophilic head of an amphiphilic molecule interacts via attraction with the aqueous phase, whereas the hydrophobic aliphatic chains prevent the molecules from being dissolved into the aqueous phase, thereby effectively reducing the interfacial free energy. In general, this phenomena is known to be less prevalent for short chain *n*-alkanes up to octane,[13,14] because these molecules have relatively high vapor pressure and chemical potential at room temperature. In consideration of this, the search for a molecule with high chirality effects is carried out within the limit of these restrictions on molecular structure.

Recently, however, several groups have revealed that even hydrophobic oils that are typically incapable of being spread on water, can form stable Langmuir monolayers on water owing to their strong internal cohesion and structural anisotropy.[15−17] In addition, the urea lipid molecules, which are not traditional amphiphilic molecules, have been reported to form a monolayer with an orientation opposite to that of alkyl chains in contact with water.[18] The advent of those nontraditional molecules as monolayer-forming species provides an opportunity to expand the scope of molecular design to optimize molecular packing

* To whom all correspondence should be addressed. E-mail: TAMURA.Kenji@nims.go.jp.
† National Institute for Materials Science.
‡ The University of Tokyo.
§ CREST, Japan Science and Technology Agency (JST).

10.1021/jp049349p CCC: $27.50
Published on Web 05/21/2004

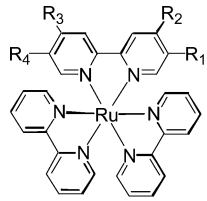

1 R_1, R_4=-H, R_2=-CH_3, R_3=-$C_{11}H_{23}$

2 R_1, R_4=-H, R_2, R_3=-$C_{11}H_{23}$

3 R_2, R_3=-H, R_1=-CH_3、R_4=-$C_{11}H_{23}$

4 R_2, R_3=-H, R_1, R_4=-$C_{11}H_{23}$

5 R_1, R_4=-H, R_2=-CH_3, R_3=-$C_{18}H_{37}$

6 R_1, R_4=-H, R_2, R_3=-$C_{18}H_{37}$

Figure 1. Structures of the investigated Ru(II) complexes.

and chirality distinction. Therefore, in consideration of this expanded approach to molecular design, this study intends to examine the chirality effect on monolayer behavior, covering traditional and nontraditional amphiphilic metal complexes.

In this study, six types of amphiphilic tris(bipyridyl)-ruthenium(II) complexes were synthesized and an attempt at resolution of these species was made. Figure 1 presents the structures of the six complexes used in the present study. Among the complexes, compounds **3** and **4** are the nontraditional amphiphiles that have mono- or dialkyl chains branching horizontally on the side of the headgroup. The polar headgroups are chiral due to the asymmetric coordination structure. This $\Delta\Lambda$-isomerism of transition metal tris-chelates bears unique steric and electronic characters, not achievable with carbon centers, which may provide a significantly new perspective of the chirality recognition in monolayers. The monolayer behavior of these complexes was studied at an air−water interface with a chloroform solution of each compound spread onto a subphase. The effects of homo- and heterochirality on molecular packing in the two-dimensional state were examined by comparison of the monolayer formation behavior of a racemic mixture and a pure enantiomer, on a subphase including a chiral molecule.

2. Experimental Section

2.1. General Procedure for the Synthesis of Amphiphilic Ruthenium(II) Complexes. The aliphatically substituted ligands L^1−L^5 were synthesized following a modified procedure from the literature.[19−24] In a typical reaction, a solution of 4,4′-dimethyl-2,2′-bipyridyl (1.00 g, 5.42 mmol) in dry THF (30 cm^3) was cooled below −40 °C under nitrogen, and a large excess of lithium diisopropylamide (LDA) (1.52 mL, 10.84 mmol) added over 30 min. After stirring at −40 °C for 3 h, a large excess of the appropriate bromoalkane (6.50 mmol) was added in dry THF (20 cm^3) and the reaction mixture was slowly warmed to room temperature while stirring overnight. The reaction was quenched with water (1−2 cm^3) and the solvent was removed in vacuo. All samples were recrystallized in ethanol several times. 4,4′-Dioctadecyl-2,2′-bipyridine (L^6) was purchased from Wako Chem. Ind.

4-Methyl-4′-undecyl-2,2′-bipyridine (L^1). Yield: 70%. ^{1}H NMR (200 MHz, $CDCl_3$/TMS): δ (ppm) = 0.88 (t, 3H, bpy−CH_2−C_9−CH_3), 1.25 (18H, bpy−CH_2−C_9(−CH_2−)−CH_3), 2.44 (s, 3H, bpy−CH_3), 2.69 (t, 2H, bpy−CH_2−C_9−CH_3), 7.13 (d, 2H, bpy-4,4′), 8.23 (s, 2H, bpy-3,3′), 8.55 (d, 2H, bpy-6,6′).

4,4′-Diundecyl-2,2′-bipyridine (L^2). Yield: 58%. ^{1}H NMR (200 MHz, $CDCl_3$/TMS): δ (ppm) = 0.88 (t, 6H, bpy−CH_2−C_9−CH_3), 1.25 (36H, bpy−CH_2−C_9(−CH_2−)−CH_3), 2.69 (t, 4H, bpy−CH_2−C_9−CH_3), 7.13 (d, 2H, bpy-5,5′), 8.22 (s, 2H, bpy-3,3′), 8.55 (d, 2H, bpy-6,6′).

5-Methyl-5′-undecyl-2,2′-bipyridine (L^3). Yield: 46%. ^{1}H NMR (200 MHz, $CDCl_3$/TMS): δ (ppm) = 0.88 (t, 3H, bpy−CH_2−C_9−CH_3), 1.28 (18H, bpy−CH_2−C_9(−CH_2−)−CH_3), 2.39 (s, 3H, bpy−CH_3), 2.65 (t, 2H, bpy−CH_2−C_9−CH_3), 7.60 (d, 2H, bpy-3,3′), 8.24 (d, 2H, bpy-4,4′), 8.48 (s, 2H, bpy-6,6′).

5,5′-Diundecyl-2,2′-bipyridine (L^4). Yield: 48%. ^{1}H NMR (200 MHz, $CDCl_3$/TMS): δ (ppm) = 0.88 (t, 6H, bpy−CH_2−C_9−CH_3), 1.28 (36H, bpy−CH_2−C_9(−CH_2−)−CH_3), 2.65 (t, 4H, bpy−CH_2−C_9−CH_3), 7.60 (d, 2H, bpy-3,3′), 8.26 (d, 2H, bpy-3,3′), 8.48 (s, 2H, bpy-6,6′).

4-Methyl-4′-octadecyl-2,2′-bipyridine (L^5). Yield: 57%. ^{1}H NMR (200 MHz, $CDCl_3$/TMS): δ (ppm) = 0.88 (t, 3H, bpy−CH_2−C_9−CH_3), 1.26 (32H, bpy−CH_2−C_9(−CH_2−)−CH_3), 2.44 (s, 3H, bpy−CH_3), 2.69 (t, 2H, bpy−CH_2−C_9−CH_3), 7.13 (d, 2H, bpy-4,4′), 8.23 (s, 2H, bpy-4,4′), 8.54 (t, 2H, bpy-6,6′).

Amphiphilic ruthenium(II) complex salts with ligands L^1−L^6 were synthesized and optically resolved according to the previous reports.[25] As a result, typically two types of molecules, $[Ru(bpy)_2(4,4'\text{-dC11bpy})]^{2+}$ and $[Ru(bpy)_2(5,5'\text{-dC11bpy})]^{2+}$, were resolved. The resolution of other compounds was not achieved in this present work. Perchlorate salts of chiral Ru(II) complexes were obtained by adding excess $NaClO_4$. The crystals were finally purified using a HPLC column (Capcel Pack, Shiseido Co. Ltd.) with a water−methanol solution as an eluent.

2.2. Instruments. Surface pressure−area (π−A) isotherms were measured with a Langmuir trough (FSD-100, USI System). The surface pressure was measured with a Wilhelmy balance. Temperature was controlled using circulating water at 20 °C. A solution of a Ru(II) complex salt was spread onto an aqueous subphase in the Langmuir trough. After 30 min, the floating film was compressed at a rate of 10 cm^2 min^{-1}. The compression−decompression procedure was repeated three times in succession.

Morphologies of monolayer at the air−water interface were observed with a Brewster angle microscope (BAM) (BM-1000, USI System). *p*-Polarized light from a 8 mW He−Ne laser (633 nm) was reflected off the air−water interface at the Brewster angle (53.1° for the air−water interface). The reflected beam passed through an analyzer fixed near 0° to the incident polarization was directed into an interference-free CCD camera. The obtained images were recorded by a DVD recorder.

X-ray reflectivity (XRR) measurements were applied to characterize a Langmuir−Blodgett (LB) monolayer film on a substrate. XRR measurements were performed with a RINT 2100 in-plane X-ray diffractometer (Rigaku), using an X-ray source (Cu Kα 1.54 Å) equipped with a graded *d*-spacing parabolic multilayered mirror, of which the optical geometry around the sample has been previously described.[26] Monolayer film samples for XRR measurements were prepared by the vertical dipping method at a dipping rate of 5 mm min^{-1} and a surface pressure of 15 mN m^{-1}, using a hydrophilic silicon wafer as the substrate. XRR was measured by scanning the tilt angle, α, of the (horizontal) sample surface with respect to the primary beam direction and by simultaneously moving the detector arm by 2α. Thus, the scattering vector **q** only has a component vertical to the sample surface (z-direction; $qz = 4\pi/\lambda \sin \alpha$, where λ is the wavelength of radiation). Reflectivity, *R*, the ratio of the reflected and incident beam intensities, was calculated in the kinematic approximation.[27] A box model was applied to parametrize the electron density distribution in the monolayer along the surface normal.[28] Each box with a certain length represents a region of quasi-constant density (Figure 2).

Ab initio Hartree−Fock (HF) self-consistent field molecular orbital calculations were performed using GAUSSIAN 98.[29] The geometric structures of the complexes, $[Ru(bpy)_2L^2](ClO_4)_2$ and $[Ru(bpy)_2L^4](ClO_4)_2$, were optimized at the STO-3G basis set. Energy calculations were performed using the 6-31G(d) basis

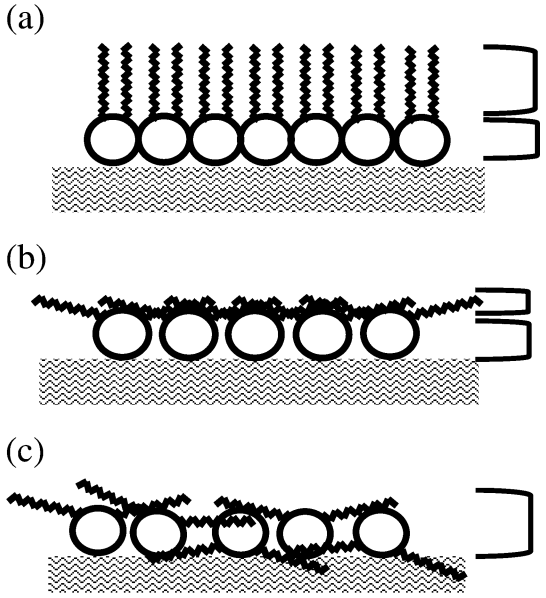

Figure 2. Schematic structure of monolayer on the air−water interface: (a) ordered structure of traditional molecules, 2-boxes model; (b) ordered structure of nontraditional molecule, 2-boxes model; (c) random structure of nontraditional molecule, 1-box model.

set. The stabilization energy, ΔE, was obtained according to the following equation:

$$\Delta E = E_{\text{total}} - E_{\text{complex}} - E_{\text{perchlorate}}$$

where E_{total}, $E_{\text{complex,}}$ and $E_{\text{perchlorate}}$ denote the total energies of the three-ion interaction system, a complex cation and two perchlorate anions, respectively. The calculated stabilization energy was corrected for the basis set superposition error.

3. Results and Discussion

3.1. Monolayer behaviors on a subphase of 0.1 M $NaClO_4$. Figure 3 summarizes the results of $\pi-A$ isotherms for a chloroform solution of a racemic mixture compound spread onto a 0.1M $NaClO_4$ aqueous solution at 20 °C.

Figure 3a compares the isotherms of $[Ru(bpy)_2L^1](ClO_4)_2$ (**1**) and $[Ru(bpy)_2L^2](ClO_4)_2$ (**2***)*, which possess one and two undecyl groups at the 4- and 4,4′-positions in the bpy ligand, respectively. The isotherms display a lift-off area at 1.10 and 1.27 nm^2 $molecule^{-1}$, respectively. Further compression resulted in the surface pressure gradually rising to 28 and 38 mN m^{-1}, respectively, followed by a sudden decrease, indicating the collapse point of the floating monolayers.

Figure 3b compares the isotherms of $[Ru(bpy)_2L^3](ClO_4)_2$ (**3**) and $[Ru(bpy)_2L^4](ClO_4)_2$ (**4**), which possess one and two undecyl groups at the 5- and 5,5′-positions in the bpy ligand, respectively. The isotherms display a lift-off area at 1.25 and 1.65 nm^2 $molecule^{-1}$, respectively. The surface pressure increased steeply until a plateau was reached above 20 mN m^{-1}, at an equilibrium of spreading pressure. The plateaus continued to a molecular area as low as 0.5 nm^2 $molecule^{-1}$.

Figure 3c compares the isotherms of $[Ru(bpy)_2L^5](ClO_4)_2$ (**5**) and $[Ru(bpy)_2L^6](ClO_4)_2$ (**6**), which possess one and two octadecyl groups at the 4- and 4,4′-positions in the bpy ligand, respectively. The isotherms display a lift-off area at 1.06 and 1.62 nm^2 $molecule^{-1}$, followed by a gradual rise in surface pressure up to 41 and 32 mN m^{-1} at 0.43 and 0.79 nm^2 $molecule^{-1}$, respectively. Beyond these surface pressures, the isotherms showed a decline, representing the collapse of the monolayers.

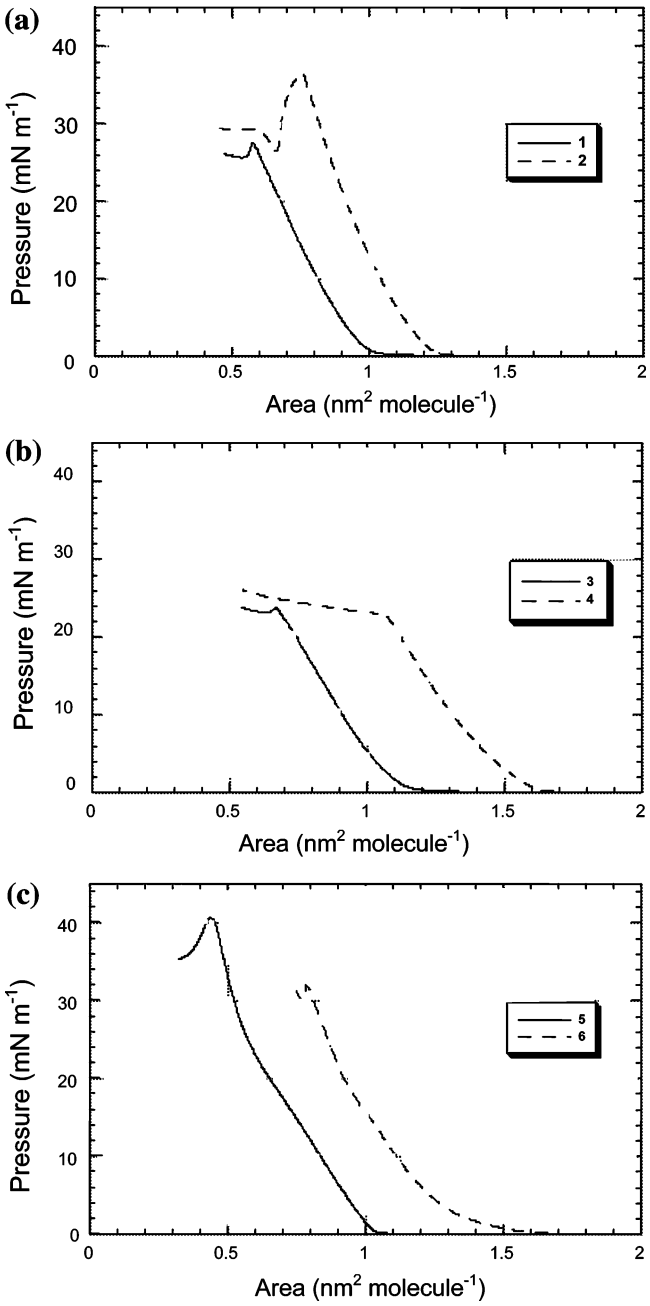

Figure 3. $\pi-A$ isotherms for floating monolayers of racemic Ru(II) complexes spread on 0.1 M $NaClO_4$ aqueous solution at 20 °C: (a) *rac*-$[Ru(bpy)_2L^1](ClO_4)_2$ (**1**), *rac*-$[Ru(bpy)_2L^2](ClO_4)_2$ (**2**); (b) *rac*-$[Ru(bpy)_2L^3(ClO_4)_2$ (**3**), *rac*-$[Ru(bpy)_2L^4](ClO_4)_2$ (**4**); (c) *rac*-$[Ru(bpy)_2L^5]$-$(ClO_4)_2$ (**5**), *rac*-$[Ru(bpy)_2L^6](ClO_4)_2$ (**6**).

The most pronounced aspect of the above results is the increase of the lift-off area (or expansion of the monolayer) when the number of attached alkyl groups is varied from one to two. The increase of the lift-off area was dependent on the substitution positions and length of alkyl chains, that is, (a) 0.17, (b) 0.40, and (c) 0.56 nm^2 $molecule^{-1}$, respectively. The increase of the lift-off area is thought to be due to the steric hindrance among the attached alkyl chains at the air−water interface. It should be also noted that the observed lift-off areas in the isotherms for compounds with two alkyl chains were much larger than the geometric area of the headgroup of $[Ru(bpy)_2L]^{2+}$ (approximately 1.0 nm^2). This suggests that these molecules formed a monolayer with two alkyl chains lying flat on the air−water interface. In contrast, the lift-off areas in the isotherms of compounds with one alkyl chain were nearly equal to the

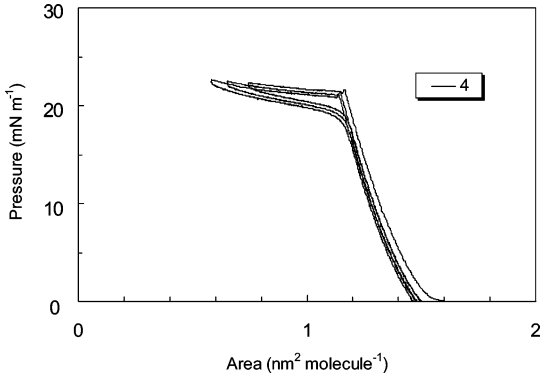

Figure 4. Compression and decompression isotherms of the *rac*-$[Ru(bpy)_2L^4](ClO_4)_2$ monolayer.

headgroup area. This suggests that these molecules oriented the alkyl chains upward from the water surface.

Another noteworthy observation is the effect of the substitution positions of the alkyl chains on the maximum surface pressure attained. That is, the compounds with 4,4′-substituted bpy ligands reached the collapse point of the monolayers after a monotonic increase of surface pressure, whereas the compounds with 5,5′-substituted bpy ligands were characterized by the appearance of plateau regions in the $\pi-A$ isotherms. The presence of such plateau regions was interpreted as being indicative of the monolayer undergoing a phase transition. To clarify this phase behavior, the compression−decompression studies were performed for the monolayer of compound **4**. As shown in Figure 4, the isotherm was reproducible for three continuous repetitions of the expansion and compression cycle. The decompression isotherm nearly coincided with the compression isotherm, except that the surface pressure was slightly lowered at the plateau region during a barrier returning. This reflected the presence of a slow reorganization process on the expansion of the monolayer surface. The slight shift toward a lower molecular area in the initial part of the $\pi-A$ isotherms could be ascribed to either dissolution of the material into the subphase or the occurrence of molecular reorganization leading to multilayer structures.

In contrast to this, the compression−decompression measurement of compound **2** revealed that the isotherm was significantly displaced toward a smaller molecular area (not shown). The second and third compression curves were displaced even further. The results indicated that compound **2** did not form a reversible monolayer.

The BAM images of the air−water interface were measured on compressing a trough surface after spreading an 80 μL chloroform solution of compound **4** (12.9×10^{-5} M) onto a subphase of 0.1 M $NaClO_4$ aqueous solution at 20 °C. Parts **a**−**c** of Figure 5 are the surface images at a surface pressure of 0 mN m^{-1} (1.9 nm^2 $molecule^{-1}$), 20 mN m^{-1} (1.2 nm^2 $molecule^{-1}$) and 27 mN m^{-1}(0.5 nm^2 $molecule^{-1}$), respectively. There was no bright domain observed on the surface at zero surface pressure (Figure 5a). Small islands could be identified in the topography with increasing surface pressure above 5 mN m^{-1} (Figure 5b). This indicated that the compound had already started to aggregate at this relatively low surface pressure. When compressed to a higher surface pressure, corresponding to the plateau region of the isotherm, the small islands were united to form larger aggregates (Figure 5c). The infrequent bright islands suggested a rough surface of the floating monolayer. On decompressing the surface from a surface pressure of 27 mN m^{-1}, it was clearly seen that the aggregates spontaneously faded out as the surface pressure approached a zero value. The plateau

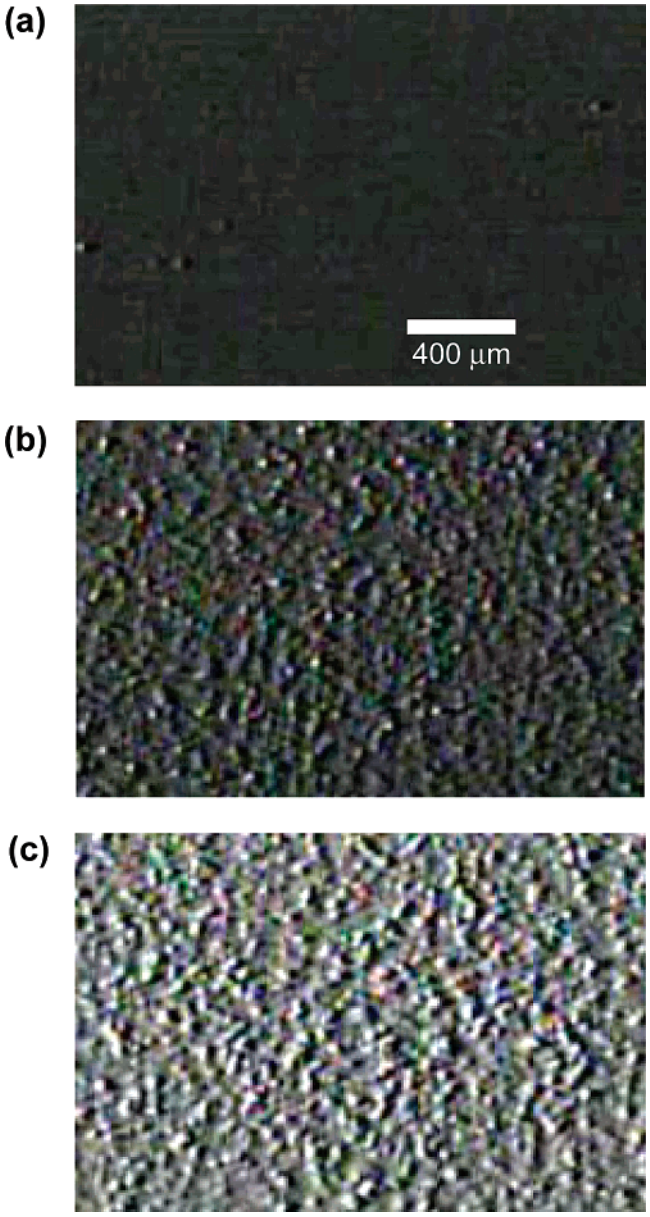

Figure 5. Brewster angle microscopy images of the *rac*-$[Ru(bpy)_2L^4](ClO_4)_2$ monolayer on the 0.1 M $NaClO_4$ aqueous solution at different compression stages: (a) 0 mN m^{-1}; (b) 20 mN m^{-1}; (c) 27 mN m^{-1}.

continued until the molecular areas became as small as 1.2−0.3 nm^2 $molecule^{-1}$. The monolayer was thought to convert into a multilayer at such a compressed state. The reversible formation of aggregates in the plateau suggests that the multilayer may be a fluidlike phase. This behavior was quite similar to the monolayer phase transition described in previous reports.[15,30]

3.2. X-ray Reflectivity (XRR) Analyses. The internal structures of LB films were investigated by XRR measurements. Figure 6 shows the XRR data for single LB films deposited onto a silicon wafer for compounds **1**−**6**. Solid curves represent the experimental data, and the theoretical fitting profiles, described below, are represented with symbols. In all of the samples, Kiessig fringes were clearly observed in the reflectivity curves, which confirmed the layered structure of the films.

The theoretical fitting profiles were analyzed with the fitting program RGXR Version 1.4 (Rigaku) based on X-ray reflection theory developed by Parratt[31] and Nevot and Croce[32] with the three parameters layer density, layer thickness, and surface roughness. Assuming the fundamental structures of films as

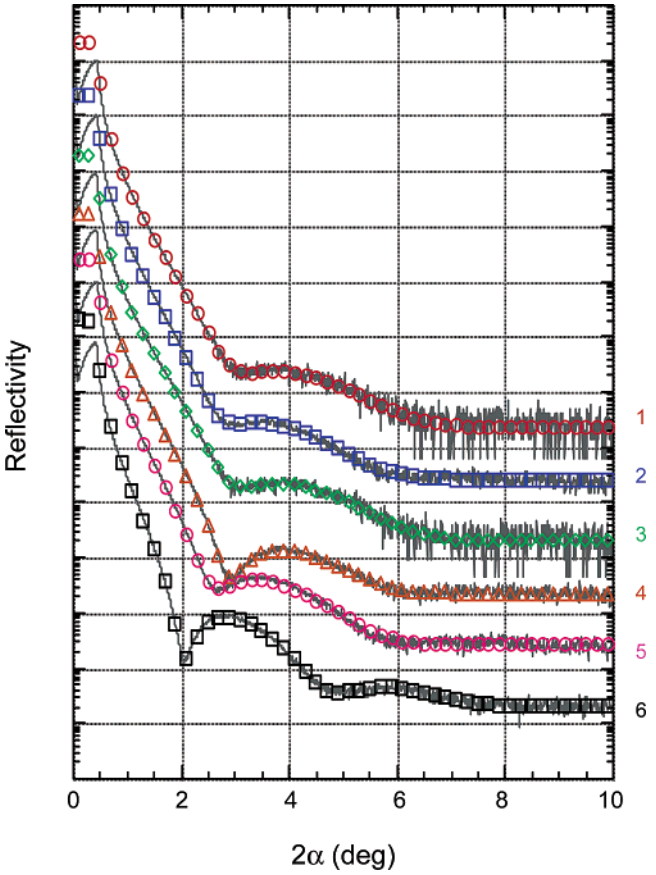

Figure 6. Experimental (solid lines) and calculated (open symbols) X-ray reflectivity curves for the monolayers of complexes transferred onto silicon substrate. The open symbols show the best data fit based on the adequate model: (**1**) one-box model; (**2**) one-box model; (**3**) one-box model; (**4**) one-box model; (**5**) one-box model; (**6**) two-box model.

TABLE 1: Layer Density, Layer Thickness, and Surface Roughness Obtained from Fitted X-ray Reflectivity (XRR) Data for the LB Monolayers on a Silicon Substrate

sample	model type	layer section	density (g/cm^3)	thickness (nm)	roughness (nm)
1	1-box		1.5	1.1	0.42
2	1-box		1.6	1.2	0.53
3	1-box		1.4	1.1	0.42
4	1-box		1.3	1.2	0.49
5	1-box		1.3	1.4	0.51
6	2-boxes	tail	1.0	1.6	0.40
		head	1.6	0.6	0.31

depicted in Figure 2, an attempt was made to reproduce the experimental curves by applying either one- or two-box models with various fitting parameters.[27] The optimum fitting parameters for each layer are given in Table 1, where the experimental results are in good agreement with the theoretical fitting curves.

For the LB films of compounds **1**−**5**, it was possible to fit the reflectivity data satisfactorily, using a one-box model. The analyses confirmed the disordered structure in these transferred monolayers, within the limits of the chosen monolayer model and the experimental accuracy of the reflectivity data. All thickness data are consistent with the values estimated from the molecular size. In Figure 6, the reflectivity curve for compound **4** was similar to, but much clearer than, those of other compounds having the same alkyl chains of C11. The clear Kiessig fringe of compound **4** implies that the LB monolayer has an extremely uniform layer structure on a horizontal plane.

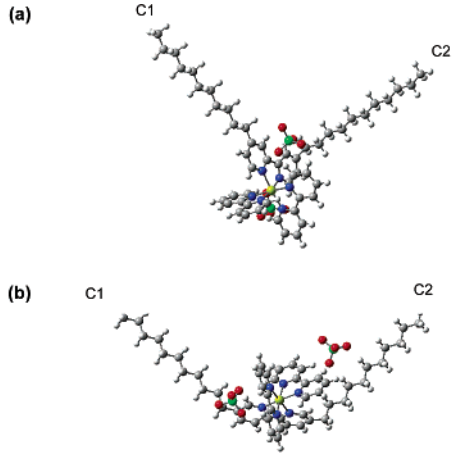

	C1-C2 length (nm)	∠C1-Ru-C2 (deg)	ΔE (eV)
$Ru(bpy)_2L^2$	2.54	88	
$Ru(bpy)_2L^2(ClO_4)_2$	2.49	86	-5.49
$Ru(bpy)_2L^4$	3.12	128	
$Ru(bpy)_2L^4(ClO_4)_2$	2.83	119	-5.37

Figure 7. Molecular structures of (a) $[Ru(bpy)_2L^2](ClO_4)_2$ and (b) $[Ru(bpy)_2L^4](ClO_4)_2$, optimized with ab initio calculation (STO-3G). The calculated structural parameters are listed at the bottom.

In contrast to the above molecules, the reflectivity curve of compound **6** was poorly simulated by a one-box model with a small range of fitting parameters. Therefore, the LB film of compound **6** was split into two boxes, one corresponding to a part of the $[Ru(bpy)_2L^6](ClO_4)_2$ head and the other to the L^6's alkyl chains (Figure 2a). This model has six free parameters for one LB layer on a silicon substrate: two thickness, two density, and two interface roughness parameters (Table 1). This analysis clearly demonstrates the presence of a layered structure consisting of a hydrophobic CH_2 layer and a hydrophilic head layer, with uniformity of the film. The thickness of the hydrophobic tail (1.6 nm) and the hydrophilic head (0.6 nm) were determined, and were consistent with the value of the molecule size, considering the assumed roughness.

3.3. Structure Simulations of $[Ru(bpy)_2L^2](ClO_4)_2$ and $[Ru(bpy)_2L^4](ClO_4)_2$. Parts a and b of Figure 7 show the optimized structures for compounds **2** and **4**, respectively. The calculated structural parameters are given in the inset. The calculation suggests that the hydrophilic head of $[Ru(bpy)_2L]$ is surrounded by two perchlorate anions in both cases. The C1−C2 distances between the tops of two alkyl chains (as indicated in the figures) changed from 2.53 to 2.49 nm for compound **2** and from 3.12 to 2.83 nm for compound **4**, respectively, when the complex cations were associated with two perchlorate anions. In addition, it was confirmed that the change in the angle ∠C1−Ru−C2 associated with the perchlorate anions resulted in a distortion from 128° to 119° for compound **4**, whereas there was negligible change in the angle for compound **2**.

The molecular area of compound **4,** on the basis of the above optimized structure, is estimated to be about 2.6 nm^2, when it is projected along the alkyl chains. This is much larger than the measured lift-off area of 1.6 nm^2 in the $\pi-A$ isotherm. On the basis of these experimental studies, it was concluded that compound **4** formed a floating monolayer at the air−water interface with its hydrophilic head in contact with water and the two hydrophobic tails oriented toward the air. One consequence of the present theoretical simulations is that compound **4** is so strongly associated with two perchlorate anions that it

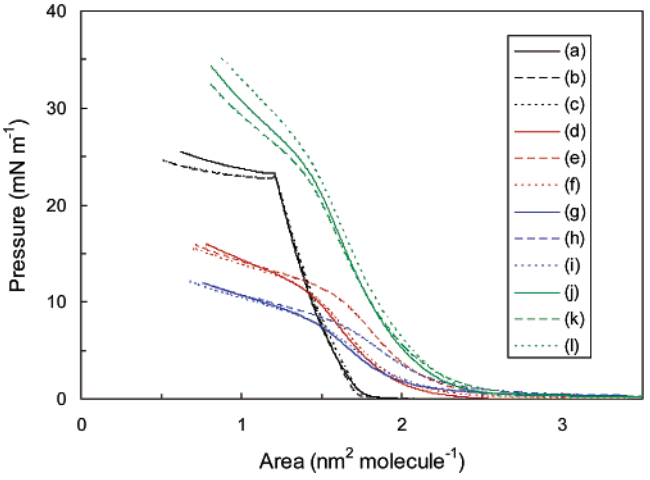

Figure 8. $\pi-A$ isotherms of racemic and enantiomeric $[Ru(bpy)_2L^4](ClO_4)_2$ monolayers on different subphases: (a)−(c) a subphase of 0.1 M $NaClO_4$; (d)−(f) a subphase of 1.0×10^{-4} M $K_2[Sb(+)\text{-}(C_4H_2O_6)]_2$; (g)−(i) a subphase of 2.5×10^{-5} M $K_2[Sb(+)\text{-}(C_4H_2O_6)]_2$; (j)−(l) a subphase of 1.0×10^{-3} M $K_2[Sb(+)\text{-}(C_4H_2O_6)]_2$; (solid line) racemic mixture of $[Ru(bpy)_2L^4](ClO_4)_2$; (broken line) Δ-isomer of $[Ru(bpy)_2L^4](ClO_4)_2$; (dotted line) Λ-isomer of $[Ru(bpy)_2L^4](ClO_4)_2$.

is regarded as a neutral molecule when forming a monolayer. If this is correct, the phase transition associated with the multilayer formation, as concluded from the $\pi-A$ isotherm, may be related to its neutrality. In other words, the cohesion energy of the molecules is sufficiently strong that the molecules undergo a reversible transformation between monolayer and multilayer states.

3.4. Chiral Discrimination by a Monolayer at the Air−Water Interface. To observe the possibility of chiral discrimination, monolayers of the racemic mixture and chiral isomers of compounds **2** and **4** were formed on an aqueous solution containing a chiral ion. Figure 8 shows the effect of $K_2[Sb_2(+)\text{-}(C_4H_2O_6)_2]$ in a subphase on the $\pi-A$ isotherms of compound **4**, in which curves a−c are the $\pi-A$ isotherms of *rac*-, Δ-, and Λ-$[Ru(bpy)_2L^4](ClO_4)_2$ on an aqueous 0.1 M $NaClO_4$ solution, respectively. The three curves were nearly identical with a lift-off area of about 1.60 nm^2 $molecule^{-1}$, indicating the homo- and heterointeractions had a negligible effect on the molecular packing in the monolayer formation. Curves d−f represent the $\pi-A$ isotherms of *rac*-, Δ-, and Λ-$[Ru(bpy)_2L^4](ClO_4)_2$ on an aqueous 1.00×10^{-4} M $K_2[Sb_2(+)\text{-}(C_4H_2O_6)_2]$ solution, respectively. In the presence of a chiral anion, $[Sb_2(+)\text{-}(C_4H_2O_6)_2]^{2-}$, the isotherms changed appreciably from those observed on a subphase of 0.1 M $NaClO_4$. The following features were noted: (1) the lift-off area increased to about 2.4 nm^2 $molecule^{-1}$ for d−f; (2) the surface pressure continued to gradually increase up to 0.4 nm^2 $molecule^{-1}$ with a slight inflection at approximately 10 mN m^{-1}; (3) the isotherm of Δ-$[Ru(bpy)_2L^4](ClO_4)_2$ (curve e) was displaced toward a larger molecular area than those of the racemic mixture and the Λ-isomer (curves d and f). As for (3), for example, the molecular area of the Δ-isomer was about 13% larger than those of the racemic mixture and the Λ-isomer at 8 mN m^{-1}. Results (3) indicated that the Λ-isomer and the racemic mixture formed a more compact monolayer than the Δ-isomer on this subphase. These results provide evidence that the $[Ru(bpy)_2L^4]^{2+}$ molecule in the monolayer state interacts stereoselectively with a chiral anion at the air−water interface or that the Δ-isomer interacts more strongly with $[Sb_2(+)\text{-}(C_4H_2O_6)_2]^{2-}$ than the Λ-isomer.

To see the effect of the concentration of a chiral anion in the subphase, the $\pi-A$ isotherms were measured after changing the concentration of $K_2[Sb_2(+)\text{-}(C_4H_2O_6)_2]$ from 2.5×10^{-5} to 1.0×10^{-3} M. Curves g−i represent the isotherms for *rac*-, Δ-, and Λ-$[Ru(bpy)_2L^4](ClO_4)_2$, respectively, for the subphase containing 2.5×10^{-5} M of $K_2[Sb_2(+)\text{-}(C_4H_2O_6)_2]$. It was shown that the surface pressure decreased when the concentration of $K_2[Sb_2(+)\text{-}(C_4H_2O_6)_2]$ decreased, whereas the stereoselectivity, indicated by (3) was still observed. On the other hand, with a higher concentration of the $K_2[Sb_2(+)\text{-}(C_4H_2O_6)_2]$ subphase (e.g., 1.0×10^{-3} M), the three isotherms for *rac*-, Δ-, and Λ-$[Ru(bpy)_2L^4](ClO_4)$ were nearly identical (curves j−l), indicating that $K_2[Sb_2(+)\text{-}(C_4H_2O_6)_2]$ was bound to the monolayers irrespective of the chirality of compound **4**.

The above difference in the isotherms (d−f and g−i) could be attributed to the preferential diastereomeric interaction between the floating Ru(II) complexes and $K_2[Sb_2(+)\text{-}(C_4H_2O_6)_2]$ in the subphase. It is noted that this selectivity was identical with that observed when $[Ru(bpy)_2L^4](ClO_4)_2$ was resolved in a methanol−water solvent system. Therefore, the same chiral recognition mode was operative in both the homogeneous phase and at the interface. As stated in the structure simulation discussion, compound **4** is expected to behave as a neutral molecule. Therefore the association with a chiral anion may be caused by the inclusion of a chiral anion into the hydrophobic region of the Ru(II) complex. Such an interaction is expected to be sensitive to the molecular shape of the anion in addition to electrostatic interactions between oppositely charged ions. It is thought that this steric effect is a main factor in the manifestation of a chirality effect toward anion association by this molecule.

In a similar experiment for compound **2**, no stereoselectivity was observed; that is, the racemic mixture and enantiomers produced the same $\pi-A$ isotherms within the experimental error (not shown).

Another aspect of the stereoselectivity exhibited by compound **4** may be related to the "liquidlike properties" of its monolayer state. As already seen in Figures 3 and 4, the monolayer of compound **4** has a unique feature in that, by compressing the monolayer, it attains the plateau region where the surface pressure is constant at approximately 20 mN m^{-1}. According to the BAM images, the molecules formed an aggregate of a few microns in this region. In the aggregates, the molecules were thought to form a multilayer with their alkyl chains extended horizontally at the interface. Such properties are thought to be intrinsic to the nontraditional structure, because the two alkyl chains of this molecule are oriented horizontally. According to the structural optimization in the ab initio calculation, both of the alkyl chains were curved slightly upward (Figure 7b), implying that compound **4** was sufficiently flexible to change its conformation according to the electrostatic interaction with the counteranions. This flexibility of the molecule may play an important role in the chiral recognition process, by allowing the system to assume a more stable configuration. This type of molecular recognition can be described as an exo-receptor function of an amphiphilic complex.

4. Conclusions

The structure−property relations of various amphiphilic ruthenium(II) complex monolayers on subphases containing different kinds of ions have been studied. Surface pressure−area isotherm measurements, Brewster angle microscopy, and X-ray reflectivity measurement have been employed in this work. As a result, $[Ru(bpy)_2L^4](ClO_4)_2$ on a subphase of aqueous $NaClO_4$ solution forms a reversible monolayer at the air−water

interface with a "plateau region". The isotherm, in which the molecules of the film are loosely packed at all $\pi > 0$, indicated that the monolayer undergoes a transition from a liquid-expanded (LE) to a metastable phase (continuous plateau region). These phenomena are clearly distinguishable from other traditional molecules. Additionally, enantiomeric and racemic $[Ru(bpy)_2L^4](ClO_4)_2$ complexes exhibited different isotherms on a subphase containing $K_2[Sb_2(+)\text{-}(C_4H_2O_6)_2]$, indicating that chiral recognition is readily detectable by the monolayer method used ($\pi-A$ measurements). The Δ-isomer of this complex displayed stronger interactions with $[Sb_2(+)\text{-}(C_4H_2O_6)_2]^{2-}$ than the Λ-isomer. In conclusion, the chiral molecular recognition mode was found to be strongly related to a preferential interaction due to the diastereomeric effect.

Acknowledgment. This work has been supported by CREST of JST (Japan Science and Technology Agency). This work has been financially supported by a Grant-in-Aid for Scientific Research on Priority Areas (417) from the Ministry of Education, Culture, Sports, Science, and Technology (MEXT) of the Japanese Government. Thanks are also due to Prof. Haruyuki Nakano (Kyushu University, Japan) and Prof. Kanta Ono (KEK, Japan) for their comments on the use of Gaussian 98.

References and Notes

(1) (a) Arnett, E. M.; Thompson, O. *J. Am. Chem. Soc.* **1981**, *103*, 968. (b) Harvey, N. G.; Mirajovsky, D.; Rose, P. L.; Verbiar, R.; Arnett, E. M. *J. Am. Chem. Soc.* **1989**, *111*, 1115. (c) Heath, J. G.; Arnett, E. M. *J. Am. Chem. Soc.* **1992**, *114*, 4500.

(2) Okamoto, T.; Yamaguchi, I. *J. Phys. Chem. B* **2003**, *107*, 10321.

(3) Okamoto, K.; Tamura, K.; Takahashi, M.; Yamagishi, A. *Colloid Surf. A* **2000**, *169*, 241.

(4) Richardson, T.; Roberts, G. G.; Polyska, M. E. C.; Davis, S. G. *Thin Solid Films* **1989**, *179*, 405.

(5) Umemura, Y.; Yamagishi, A.; Schoonheydt, R.; Persoons, A.; Schryver, F. D. *J. Am. Chem. Soc.* **2002**, *124*, 992.

(6) Kotov, N. A.; Dèkàny, I.; Fendler, J. H. *J. Phys. Chem*. **1995**, *99*, 13065.

(7) Capan, R.; Richardson, T. H.; Lacey, D. *Thin Solid Films* **2002**, *415*, 236.

(8) Ducharme, S.; Bune, A. V.,; Blinov, L. M.; Fridkin, V. M.; Palto, S. P.; Sorokin, A. V.; Yudin, S. G. *Phys. Rev. B.* **1998**, *57*, 25.

(9) Okamoto, K.; Taniguchi, M.; Takahashi, M.; Yamagishi, A. *Langmuir* **2001**, *17*, 195.

(10) *Nanoparticlus and Nanostructured Films*; Fendler, J. H., Ed.; Wiley-VCH: Weinheim, Germany, 1998.

(11) (a) Pathirana, S.; Neely, W. C.; Myers, L. J.; Vodyanoy, V. *J. Am. Chem. Soc.* **1992**, *114*, 1404−1405. (b) Pathirana S, Neely, W. C.; Vodyanoy, V. *Langmuir* **1998**, *14*, 679.

(12) Kashiwara, S.; Takahashi, M.; Nakata, M.; Taniguchi, M.; Yamagishi, A *J. Mater. Chem.* **1998**, *8*, 2253.

(13) Pfohl, T.; Möhwald, H.; Riegler, H. *Langmuir* **1998**, *14*, 5285.

(14) Dobbs, H. *Langmuir* **2000**, *16*, 4749.

(15) Li, M. Y.; Acero, A.; Huang, Z. Q.; Rice, S. A. *Nature* **1994**, *367*, 151.

(16) Weinbach, S. P.; Weissbuch, I.; Kjaer, K.; Bouwman, W. G.; Nielsen, J. A.; Lahav, M.; Leiserowitz, L. *Adv. Mater.* **1995**, *7*, 857.

(17) Tabe, Y.; Yamamoto, T.; Nishiyama, I.; Aoki, M. K.; Yoneya, M; Yokoyama, H. *J. Phys. Chem. B* **2002**, *106*, 12089.

(18) Huo, Q.; Russev, S.; Hasegawa, T.; Nishijo, J.; Umemura, J.; Puccetti, G.; Russell, K. C.; Leblanc, R M. *J. Am. Chem. Soc.* **2000**, *122*, 7890.

(19) Zotti, G.; Zecchin, S.; Schiavon, G. *Chem. Mater*. **1999**, *11*, 3342.

(20) Seddon, K. R.; Yousif, Z. Y. *Transition Met. Chem.* **1986**, *11*, 443.

(21) Fletsher, N. C.; Nieuwenhuyzen, M.; Rainey, S. *J. Chem. Soc., Dalton Trans.* **2001**, 2641.

(22) Kelly-Basetti, B. M.; Cundy, D. J.; Pereira, S. M. *Bioorg. Med. Chem. Lett.* **1995**, *5*, 2989.

(23) Quici, S.; Cavazzini, M.; Ceragioli, S.; Montanari, F.; Pozzi, G. *Tetrahedron Lett.* **1999**, *40*, 3647.

(24) Bruce, D. W.; Holbrey, J. D.; Tajbakhsh, A. R.; Tiddy, G. J. *J. Mater. Chem.* **1993**, *3*, 905.

(25) (a) Tamura, K.; Setsuda, H.; Taniguchi, M.; Takahashi, M.; Yamagishi, A. *Clay Sci.* **1998**, *10*, 409. (b) Tamura, K.; Setsuda, H.; Taniguchi, M.; Yamagishi, A. *Langmuir* **1999**, *15*, 6915. (c) Taniguchi, M.; Ueno, N.; Okamoto, K.; Karthaus, O.; Shimomura, M.; Yamagishi, A. *Langmuir* **1999**, *15*, 7700.

(26) Takahashi, S.; Taniguchi, M.; Omoto, K.; Wakabayashi, N.; Tanaka, R.; Yamagishi, A. *Chem. Phys. Lett.* **2002**, *352*, 213-219.

(27) (a) Als-Nielsen, J.; Kjaer, K. *The Proceedings of the NATO Advanced Study Institute, Plase Transitions in Soft Condensed Matter*; Geilo, Norway, April 4−14, 1989; Plenum Publishing Corp.: New York, 1989; pp 113−137. (b) Helm, C. A.; Tippmann-Krayer, P.; Möhwald, H.; Als-Nielsen, J.; Kjaer, K. *Biophys. J.* **1991**, *60*, 1457.

(28) Polouček, P.; Pietsch, U.; Geue, T.; Symietz, Ch.; Brezesinski, G. *J. Phys. D: Appl. Phys.* **2001**, *34*, 450.

(29) Frisch, M. J.; et al. *GAUSSIAN 98*; Gaussian, Inc.: Pittsburgh, PA, 1998.

(30) Petty, M. C. *Langmuir−Blodgett films An introduction*; Cambridge University Press: Cambridge, U.K., 1996.

(31) Parratt, G. *Phys. Rev.* **1954**, *95*, 359.

(32) Nevot, L.; Croce, P. *Rev. Phys. Appl.* **1980**, *15*, 359.